Thank you very much for your time and the constructive feedback on our manuscript. We truly appreciate your positive assessment. Our detailed responses are given below.

Review of "Wildfire aerosols lofted by North American pyrocumulonimbus clouds: long-range transport and aerosol-cloud-radiative effects" by Yan Wang et al.

This study examines the transcontinental transport of aerosols emitted by extreme wildfires in North America in August 2024, focusing on the role of pyrocumulonimbus (PyroCbs) clouds in the lofting of particles and their impact on cloud properties and TOA radiation. By integrating multi-platform satellite measurements and reanalyses data, the results show that PyroCbs promote the injection of aerosols into the upper troposphere and lower stratosphere, increasing the cloud fraction and altering the microphysics properties, which leads to significant radiative anomalies at continental and transcontinental scales.

Response:

Thank you for your constructive summary and positive assessment of our work. We are pleased that the reviewer recognized the significance of our study on the transcontinental transport of wildfire aerosols and their subsequent impact on cloud microphysics and radiative forcing.

We have carefully considered the comments provided and have further strengthened the discussion on PyroCb events.

I believe this study could be a valuable addition to the literature; the topic is interesting and the analysis deserves to be reviewed by the journal. However, the current study would benefit from additional clarifications and more detailed physical explanations; addressing these points may require major revision.

Response: We sincerely thank the reviewer for the positive assessment of our work and for recognizing the significance of studying the 2024 North American wildfire aerosols. We are encouraged by your comment that this study is a "valuable addition to the literature."

We fully agree that the manuscript would benefit from more detailed physical explanations and clarifications. Accordingly, we have performed a major revision of the manuscript, focusing on deepening the mechanistic analysis of PyroCb-aerosol-cloud interactions and providing more robust physical interpretations of the observed radiative anomalies.

Major comments

a-Regarding Figure 4 (critical point raised by the CC1 comment):

I noted comment CC1 regarding a possible time lag or inconsistency between Figure 4 and the presence of PyroCbs. Given that this figure is central to the interpretation of long-range aerosol trajectories and their influence on clouds and TOA radiation, I encourage the authors to clarify this figure and provide additional context to ensure consistency with the presence of PyroCbs. A clear and well-documented identification of the fires responsible for the analyzed PyroCbs would strengthen confidence in the interpretation of the result.

Response:

We thank the reviewer for highlighting this critical point and for directing our attention to the concerns raised in Comment CC1 regarding Figure 4. We agree that establishing a clear spatiotemporal link between the specific fire events and the observed PyroCbs is essential for the interpretation of long-range aerosol trajectories.

Using the revised analysis, we confirm that no pyroCb activity is identified over the northwestern United States or southwestern Canada on 12 August 2024 (local time), consistent with the CC1's reference to the Worldwide PyroCb Information Exchange (WPIE) records. The pyroCb features discussed in the manuscript are confined at 23:50 UTC, August 13 2024, with the primary source region located over northern Alberta (Region 1 at 59.5°N, 110.4°W). The time and location of this event are consistent with the pyroCb activity formed at 00:00 UTC, August 14 on a fire at 59.4°N, 110.2°W and under the thin anvil of a regular Cb reported by WPIE.

The revised manuscript text addressing this point is provided below for clarity.

[Revised manuscript text:]

"Figure 4a-d shows GOES-16/ABI observations on 13 August, revealing two distinct regions of fire-associated deep convection over northern Alberta and northern Saskatchewan, Canada. The BT11 imagery (Figure 4a-b) highlights exceptionally cold cloud tops, with darker shading corresponding to lower temperatures and greater cloud-top altitudes, consistent with intense pyroCb convection. These features are colocated with pronounced positive BTD4-11 enhancements (Figure 4c-d), reflecting altered cloud-top radiative properties associated with smoke aerosol entrainment and reduced effective particle sizes, a characteristic microphysical signature of PyroCb as established in previous studies.

The thermally and microphysically distinct cloud tops are spatially coincident with active fire detections, providing strong observational evidence for a direct linkage between surface fire activity and the observed deep convective development. Yellow shaded areas in Figure 4c-d indicate IPCB source regions that satisfy all identification criteria and represent robust detections of pyroCb-injected air masses (Li et al., 2025). Following convective lofting, these air masses undergo sustained upper-tropospheric transport and gradual eastward advection under synoptic-scale flow, illustrating the combined roles of intense fire-driven convection and large-scale circulation in enabling long-range smoke transport across central and eastern Canada.

Based on three GOES-16 infrared channel observations in Figure 4a-d, pyroCb were identified as convective clouds anchored to the wildfire source, the specific locations of pyroCb formation were identified as the yellow regions within the overlapping areas between the black regions in the grayscale shaded map and the blue-green highlighted regions. Figure 4e-f presents the NOAA HYSPLIT forward trajectories calculated to investigate the long-range transport of air masses originating from intense IPCB regions. The trajectories indicate rapid vertical transport of air masses, followed by sustained advection in the upper troposphere and lower stratosphere (UTLS). The initial release heights were constrained using cloud vertical structures from CPR/EarthCARE observations and cloud top height information from the ATLID lidar.

At 23:10 UTC on 13 August, two IPCB source regions were identified. Forward trajectories were initialized at 8 and 11 km above ground level (AGL). Air parcels released at 8 km AGL experienced rapid vertical uplift to 9-9.5 km, consistent with strong convective injection associated with IPCB activity, whereas air masses initialized at 11 km AGL largely maintained transport altitudes above 9 km, indicating efficient entrainment into the UTLS and subsequent isentropic transport. At 23:50 UTC on 13 August, trajectories were initialized from the two established IPCB source regions and an additional developing source region at 7.5 and 10 km AGL. Pronounced vertical from 7.5 km to 6-8 km remained confined to the established IPCB regions, while air parcels released at higher altitudes at 10km were transported predominantly at around 7 km, indicating sustained mid-to-upper tropospheric transport. Vertical uplift associated with the developing source region was comparatively limited. By 06:00 UTC on 15 August, forward trajectories from multiple IPCB regions showed localized convergence and partial merging, implying coordinated airflow and plume aggregation.

Following this merging phase, the combined air masses were advected eastward large-scale synoptic circulation, crossing the North Atlantic and reaching northern and western Europe, characteristic of intercontinental UTLS transport of air masses lofted by deep pyroconvection.

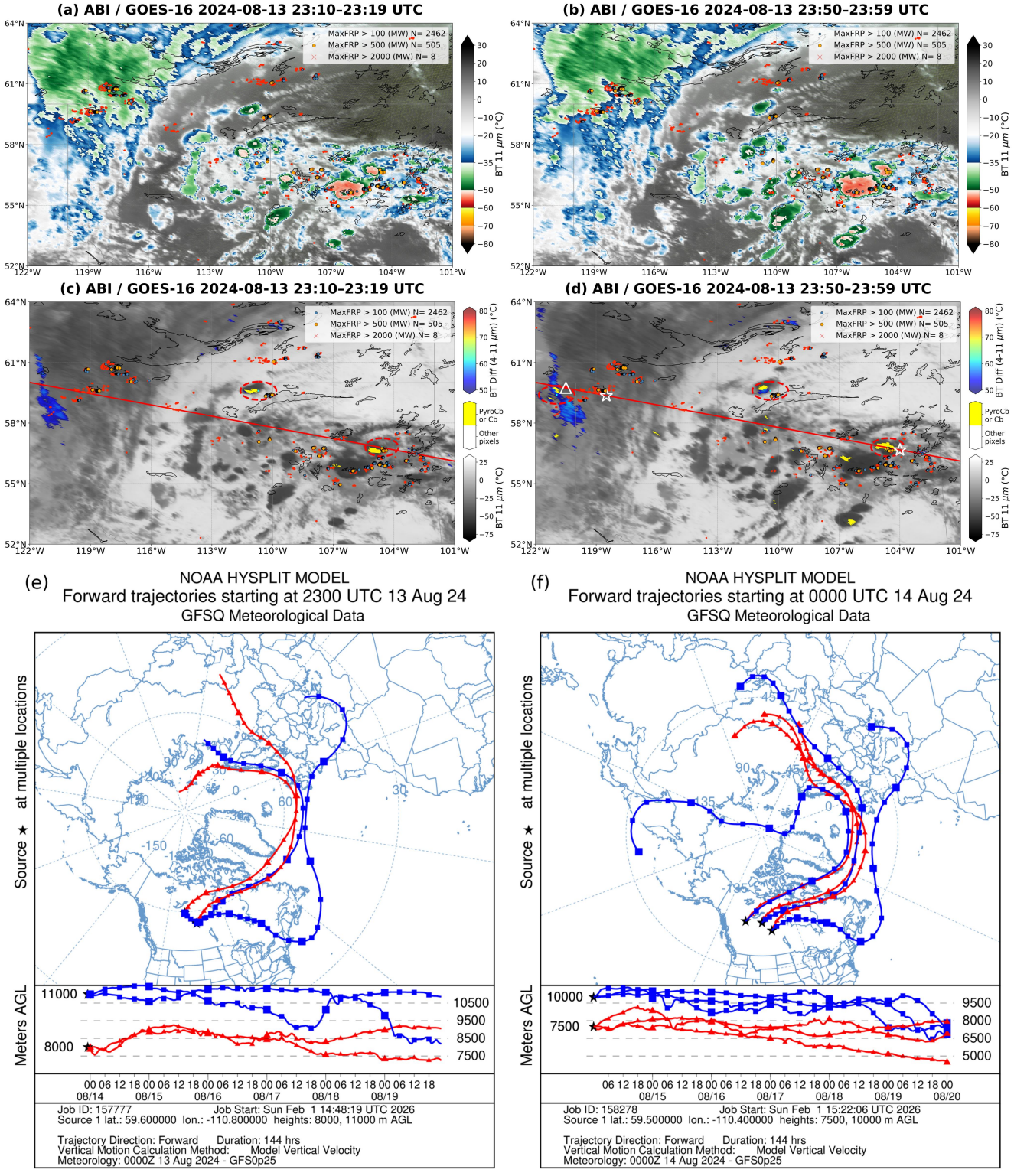

Figure 4. (Figure 1. in the revised manuscript) ABI/GOES-16 observations of cloud-top evolution and smoke transport associated with the 13 August 2024 North American pyroCb events. (a-b) Brightness temperature at 11 μm (BT11) and (c-d) brightness temperature difference between 4 and 11 μm (BTD4-11) derived from GOES-16/ABI on 13 August 2024. Red dots denote MOD14A1 active fire detections, and yellow shaded areas indicate the identified intense pyrocumulonimbus (IPCB)

source regions. The pink circle represents the 50 km radius used for pyroCb statistical analysis, with the cyan dot marking the circle center. Red lines show the cross-sections on 13 August in Figure 6. White triangle and stars show vertical pressure velocities of less than -0.4 Pa s^{-1} and high CO concentrations, respectively. (e-f) NOAA HYSPLIT Forward trajectories of air parcels released from the pyroCb source regions on 13-14 August 2024 and transported to the downwind smoke conveyor region. (a,c,e) Region 1 at 59.6°N, 110.8°W and Region 2 at 56.4°N, 104.7°W, with trajectories initialized at 23:00 UTC on August 13 and arriving at the target region by 23:00 UTC on August 19. (b,d,f) Region 1 at 59.5°N, 110.4°W , Region 2 at 56.8°N, 104.6°W and Region 3 at 59.5°N, 120.95°W, with trajectories initialized at 00:00 UTC on August 14 and arriving at the target region by 00:00 UTC on August 20. "

b-Regarding the Influence of smoke aerosols on cloud formation.

The use of CERES data to study cloud microphysics is interesting, but it presents significant limitations depending on the scale and level of detail targeted. The native resolution of CERES does not allow capturing the fine gradients needed to analyze microphysical variability at the scale of individual convective clouds or PyroCb structures. Moreover, PyroCbs contain a high fraction of absorbing aerosols (BC, organic compounds), which bias the retrievals of COD and CER.

Have you considered averaging vertical profiles over the August 2024 PyroCb events (or cross validating the observed anomalies against lidar measurements) using synergistic products (e.g., EarthCARE ATLID/CPR)? Cloud property retrieval algorithms could then be applied to derive microphysical properties, thereby complementing CERES observations and improving the characterization of cloud altitude, optical thickness, and structure.

Response:

We thank the reviewer for this insightful comment. We fully agree that the coarse resolution of CERES and the presence of absorbing aerosols (such as Black Carbon and organic compounds) in PyroCbs can introduce uncertainties in retrieving cloud microphysical properties, particularly Cloud Optical Depth (COD) and Cloud Effective Radius (CER).

To address this concern and cross-validate the CERES observations as suggested, we have conducted a pixel-to-pixel inter-comparison using high-resolution synergistic products from EarthCARE (ATLID and CPR) and PACE (HARP2), as shown in Figure A1. We focused on the August 2024 PyroCb events and analyzed two distinct scenarios of the same region: "Wildfire" and "No Wildfire". The validation results indicate that CERES CTH retrievals show good consistency with the EarthCARE ATLID lidar measurements, with small biases, confirming that CERES effectively captures the vertical extent of the PyroCb structures. As expected, the presence of absorbing aerosols introduces some uncertainty in CER and COD retrievals. The

Root Mean Square Errors (RMSE) for CER and COD are approximately 3 and 5 µm, respectively, compared to the synergistic EarthCARE product. While biases existing, these uncertainties fall within the threshold requirements defined by GCOS, especially considering the complexity of cloud monitoring under extreme aerosol loading conditions.

Crucially, to mitigate the impact of absolute retrieval biases, our study focuses on spatial anomalies (Δ) relative to the multi-year climatology (as shown in Figure 7 in the manuscript), rather than absolute magnitudes. The PyroCb-induced perturbations represent a strong signal that significantly exceeds the retrieval noise quantified above. By analyzing the deviation from the climatological mean, we isolate the intense cloud disturbances triggered by the wildfires. Even if smoke aerosols induce a systematic bias in the absolute retrieval, the relative spatial pattern and the magnitude of the anomaly remain robust indicators of the PyroCb impact. Therefore, while we interpret the absolute microphysical values with caution, the relative trends and the identification of significant anomalies presented in the manuscript are statistically significant and physically consistent with the lidar cross-validation.

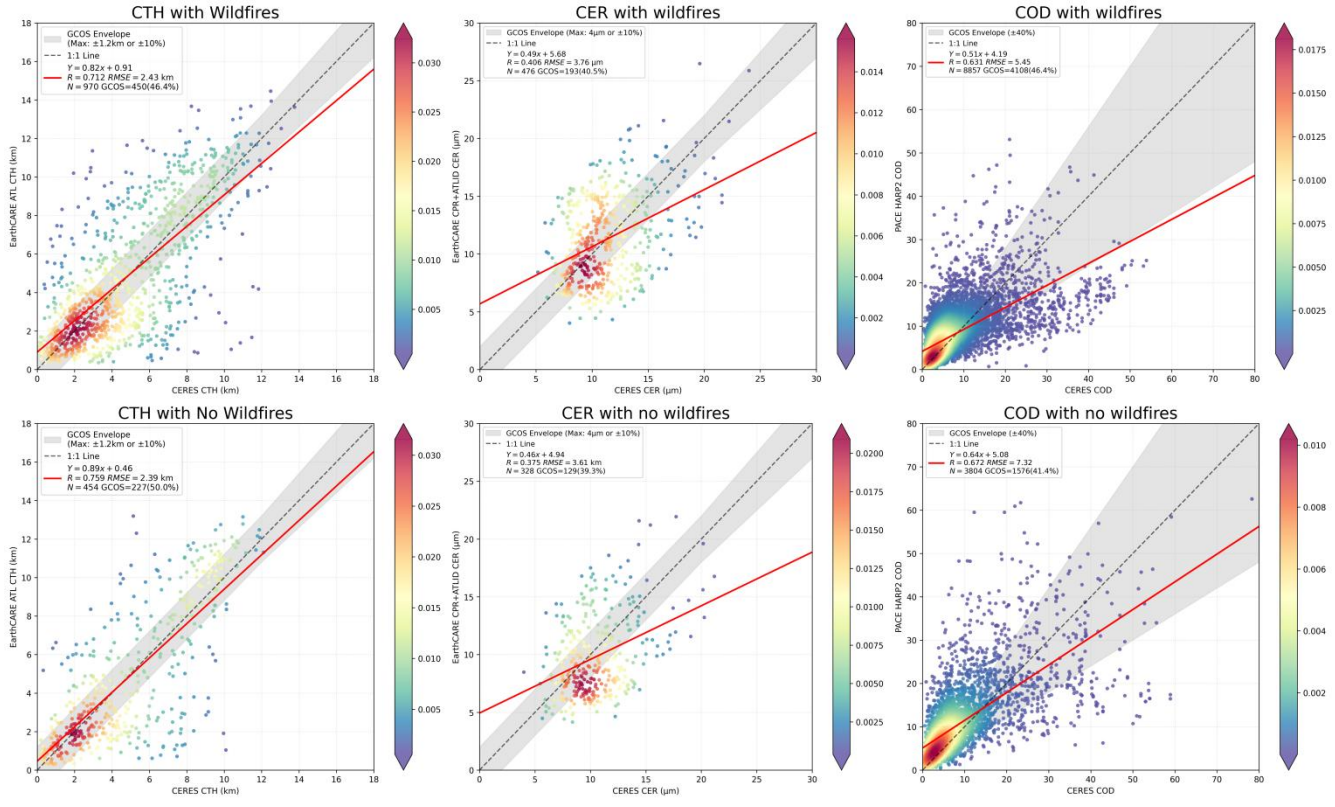

Figure A2. Inter-comparison of CERES cloud property retrievals against high-resolution active (EarthCARE) and multi-angle passive (PACE) sensors during the August 2024 PyroCb events. To assess potential biases caused by absorbing aerosols and resolution limitations, pixel-to-pixel comparisons were performed for Wildfire (top row) and No Wildfire (bottom row) scenarios. Columns from left to right display comparisons for: (1) Cloud Top Height (CTH) between CERES and ATLID/EarthCARE; (2) Cloud Effective Radius (CER) between CERES and EarthCARE

synergistic product (CPR+ATLID); and (3) Cloud Optical Depth (COD) between CERES and HARP2/PACE.

The conclusion in lines 470–475 is unclear because 4-day delay between the CCN increase (6–11 August) and the subsequent rise in cloud fraction (11–14 August) does not appear consistent with the Twomey or Albrecht effects, which are primarily microphysical processes acting on cloud-formation timescales (minutes to hours or a day). Such a multi-day lag instead suggests that the cloud response is largely governed by dynamical and meteorological processes, rather than by immediate microphysical aerosol–cloud interactions alone.

Response:

We thank the reviewer for this insightful comment regarding the timescale of aerosol – cloud interactions. We agree that the multi-day lag between the enhancement in CCN concentration on 6–11 August and the gradual increase in cloud fraction on 10–14 August is inconsistent with the characteristic timescales of the Twomey or Albrecht effects, which primarily operate on short (minutes to hours or a day) microphysical timescales.

In the revised manuscript, we have clarified this distinction and revised the discussion accordingly. The simultaneous increase in CCN concentration and reduction in aerosol effective radius are now interpreted as evidence of a rapid microphysical adjustment consistent with the Twomey effect. In contrast, the subsequent increase in cloud fraction is attributed primarily to evolving large-scale dynamical and meteorological conditions. We further note that aerosol-induced microphysical changes may have preconditioned the cloud environment, potentially modulating the cloud response under favorable dynamical conditions, rather than acting as the sole driver of cloud fraction changes. These revisions clarify the respective roles of microphysical aerosol effects and dynamical processes and address the reviewer's concern regarding the interpretation of the observed temporal lag.

The revised manuscript text addressing this point is provided below for clarity.

[Revised manuscript text:]

"*During the active fire period (6 – 11 August), we observed a simultaneous increase in CCN concentration, accompanied by a reduction in effective radius. These variations are radiatively significant, as the combination of smaller effective radii and optically thicker clouds enhances cloud*

albedo. This increased reflectivity directly contributes to the instantaneous negative radiative forcing observed at the Top of Atmosphere (TOA). We focus here on these resulting radiative impacts, which are robustly supported by the satellite observations."

Similarly, the conclusion in lines 674–675—"the cloud response is evident from the CERES-derived ΔCTH, ΔCOD, and ΔCER anomalies and is consistent with aerosol–cloud interactions and the Twomey effect"—may be somewhat strong. Relying exclusively on CERES data, without cross-validation using active remote sensing observations (e.g., lidar) to disentangle microphysical aerosol effects from dynamical forcing, makes the attribution to the Twomey effect less certain.

Response:

We thank the reviewer for this valuable comment and agree that the original wording may have overstated the attribution to the Twomey effect. We acknowledge that CERES-derived cloud property anomalies (ΔCTH, ΔCOD, and ΔCER), while providing important information on cloud microphysical changes, are based on passive radiometric observations and therefore cannot fully disentangle aerosol microphysical effects from concurrent dynamical and meteorological influences.

To address this, we have revised the conclusion to adopt a more cautious tone. We no longer claim the response is "evident" but rather that the observed anomalies align with the characteristics of the Twomey effect, while acknowledging that these observations suggest potential microphysical interactions rather than serving as absolute proof.

The revised manuscript text addressing this point is provided below for clarity.

[Revised manuscript text:]

"The variations in ΔCTH, ΔCOD, and ΔCER observed from CERES resemble the patterns associated with the Twomey effect, supporting the hypothesis of aerosol-induced microphysical changes, although dynamical contributions cannot be fully excluded."

c- Regarding the Influence of smoke aerosols on TOA radiation

The interpretation of the SW anomalies seems not fully consistent with the figures. Some statements in the text do not appear to match what is shown in Figures 10 and 11. For example, under all-sky conditions, the manuscript reports negative SW anomalies over USW, whereas the corresponding panels

seem to show positive values. Similarly, positive anomalies reported over NA, WE, and IGB are not clearly supported by Figures 10c and 11c, where negative anomalies appear to dominate in these regions. And similar with the net downward anomalies in clear sky.

Moreover, several positive and negative anomalies are visible outside the predefined study regions, which makes it difficult to attribute the reported signals uniquely to the source or transport regions discussed in the text.

Response:

We thank the reviewer for this insightful comment. We agree that distinguishing the specific smoke-induced signal from background meteorological variability is crucial for accurate attribution.

To address this concern and demonstrate the robustness of the reported signals, we have made the following three major revisions to Figures 2-5 and the corresponding analysis. We performed a Z-score analysis based on 24 years of historical climatology (2000–2023) to filter out random noise.

In the revised figures, we applied stippling to regions where the anomalies are statistically significant at the 95% confidence level ($|Z| > 1.96$). The results confirm that the reported anomalies within the study regions are statistically robust, whereas many anomalies outside these regions are not significant and likely represent natural variability. We overlaid contours of surface Black Carbon (BC) concentration and ΔAOD increases onto the TOA radiation maps. The analysis reveals a strong spatial consistency between the significant TOA radiative forcing and high aerosol loading, providing physical evidence that these specific anomalies are driven by smoke presence. We integrated the PyroCb source locations and forward HYSPLIT trajectories at 10,000 m (blue lines) and 8,000m (green lines) into the figures. The trajectories originating from the PyroCb outbreak regions closely correspond to the statistically significant TOA anomalies within the study regions. While some significant anomalies exist outside this primary transport pathway (likely driven by other synoptic systems), the co-location of the trajectories, high aerosol loading (BC/AOD), and significant TOA signals strongly supports the attribution of the reported effects to the smoke transport.

While we acknowledge the presence of some anomalies outside the primary study area, the convergence of statistical significance, high aerosol concentrations (BC/AOD), and air mass trajectories uniquely attributes the reported signals in the study regions to the transport of wildfire smoke. Anomalies outside this transport pathway that do not align with these markers

are attributed to other synoptic-scale meteorological variability.

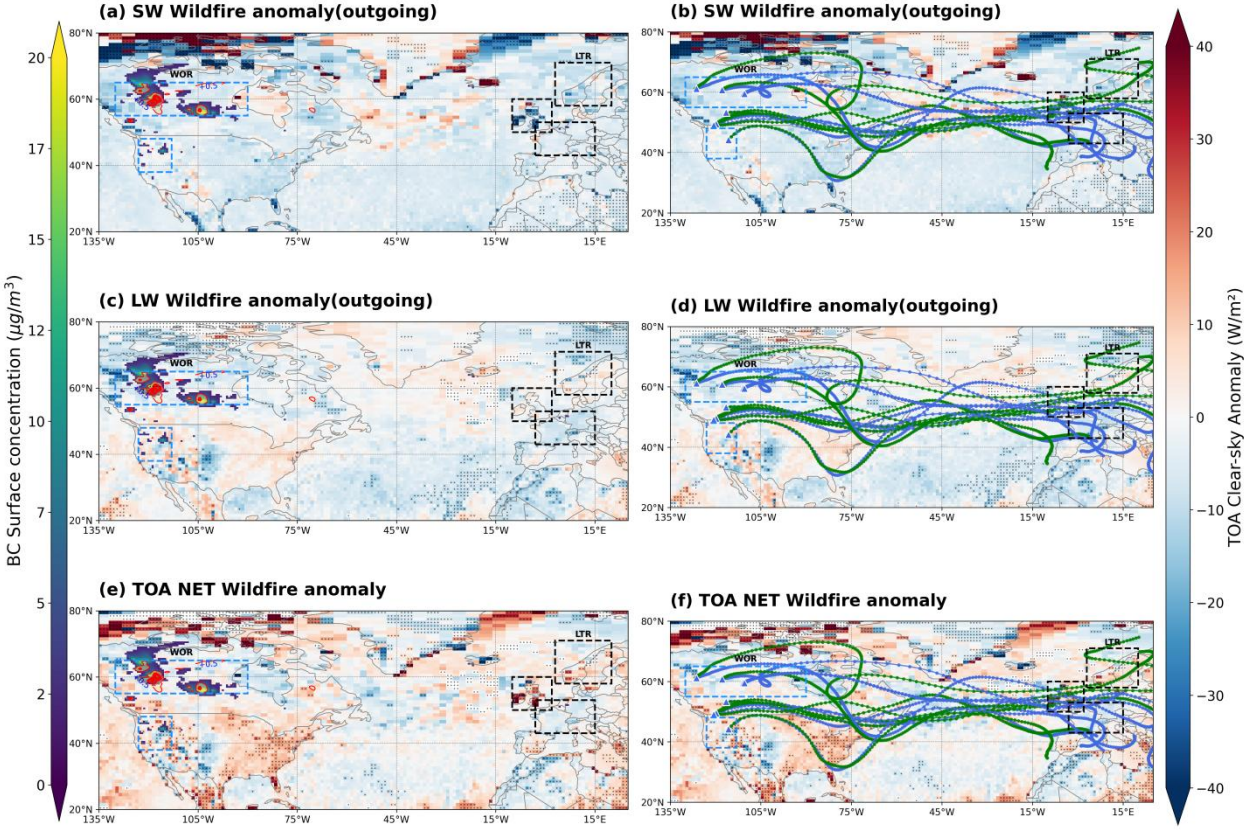

Figure A3. TOA Clear-sky radiative flux anomalies associated with wildfire events. The panels display anomalies for (a, b) Shortwave (SW), (c, d) Longwave (LW), and (e, f) Net radiation. Anomalies are calculated as the difference between the wildfire composite mean and the 24-year climatological mean, processed independently to remove seasonal variations (see Section 2.3.2). Stippling indicates regions where anomalies are statistically significant at the 95% confidence level. (a, c, e), contours represent surface Black Carbon (BC) concentrations and AOD anomalies. (b, d, f), lines indicate HYSPLIT forward trajectories initiated from the identified PyroCb source regions at 10,000 m (blue) and 8,000 m (green).

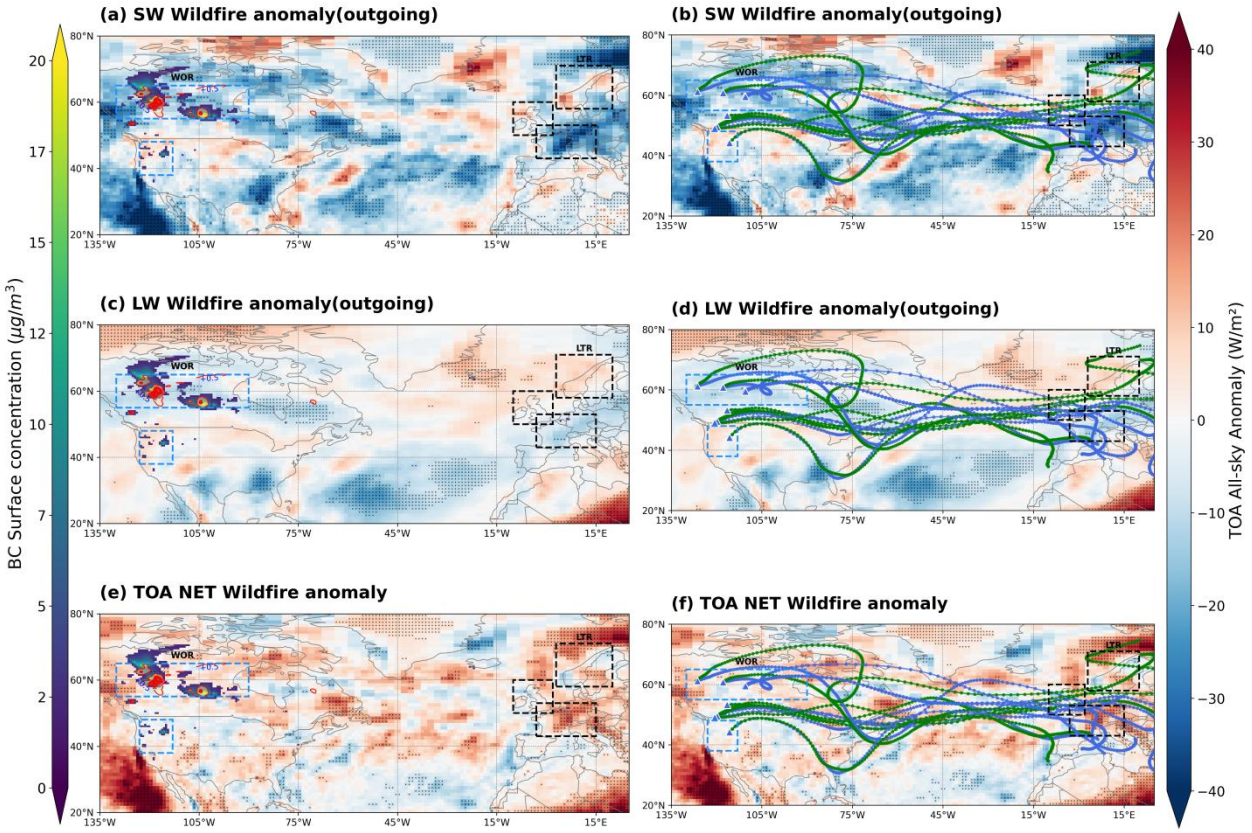

Figure A4. TOA All-sky radiative flux anomalies associated with wildfire events. The panels display anomalies for (a, b) Shortwave (SW), (c, d) Longwave (LW), and (e, f) Net radiation. Anomalies are calculated as the difference between the wildfire composite mean and the 24-year climatological mean, processed independently to remove seasonal variations (see Section 2.3.2). Stippling indicates regions where anomalies are statistically significant at the 95% confidence level. (a, c, e), Contours represent surface Black Carbon (BC) concentrations and AOD anomalies. (b, d, f), Lines indicate HYSPLIT forward trajectories initiated from the identified PyroCb source regions at 10,000 m (blue) and 8,000 m (green).

The revised manuscript text addressing this point is provided below for clarity.

[Revised manuscript text:]

"We have performed a Z-score significance test based on 20 years of historical data. In the revised Figure 10-11, stippling has been added to highlight statistically significant regions ($p < 0.05$). As shown, the signals within our study regions are densely stippled (robust), whereas the anomalies outside these regions are mostly not stippled, indicating they are within the range of natural climate variability and can be attributed to background noise.

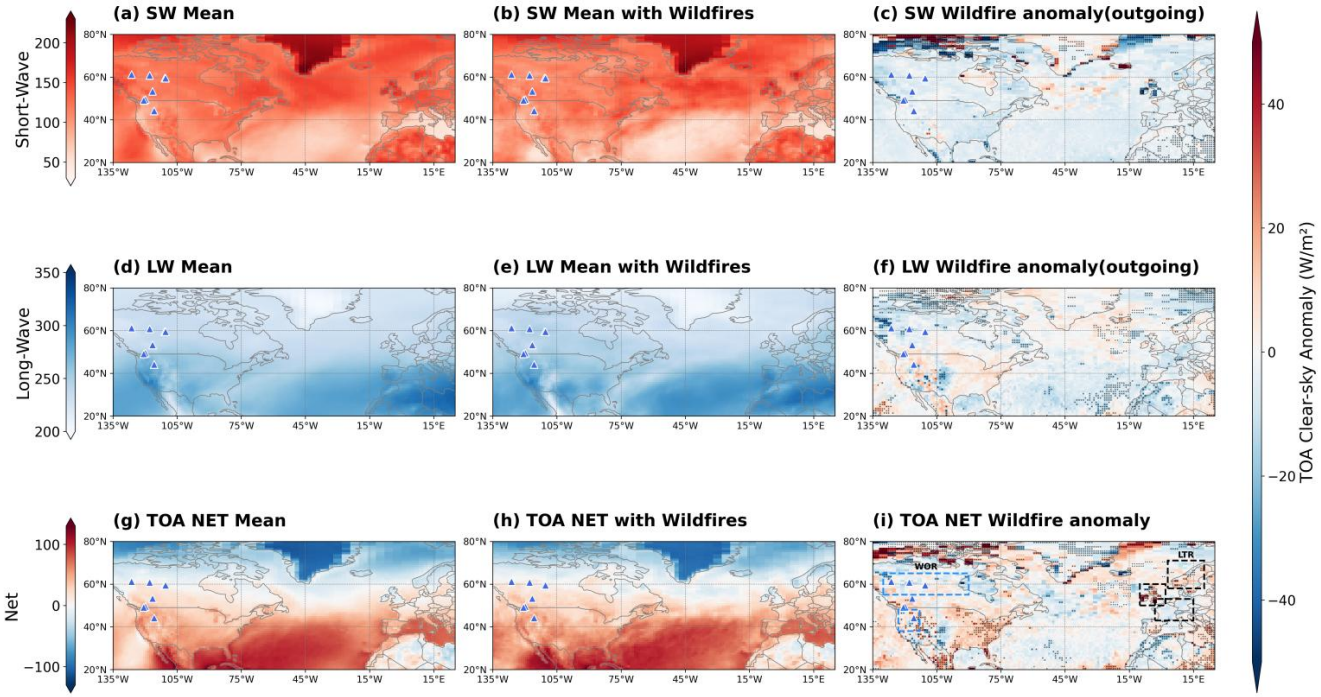

Figure 10. (Figure 5. in the revised manuscript) Wildfires are associated with Clear-sky TOA radiative Flux Changes. (a-i) Monthly climatological mean TOA radiative fluxes (a, d, g), mean TOA radiative fluxes during Wildfire events (b, e, h) and mean wildfire-associated TOA heat flux anomalies (c, f, i) for SW radiation (a-c), LW radiation (d-f) and Net radiation (g-i). A positive SW anomaly indicates increased outgoing solar radiation or reduced cloud reflection; a positive LW anomaly means more outgoing LW radiation is retained less emitted to space. Net is qualitatively by using SW and LW, but net is calculated independently to remove the seasonal effects of wildfire frequency. Anomalies represent the difference between total events and climatological mean events (Wildfires - Climatology), calculated independently to remove seasonal variations in wildfire events (see in Section 2.3.2). Stippling indicates regions where anomalies are statistically significant at the 95% confidence level based on a 24-year climatology. Blue rectangles show the spatial distribution of identified pyroCb events.

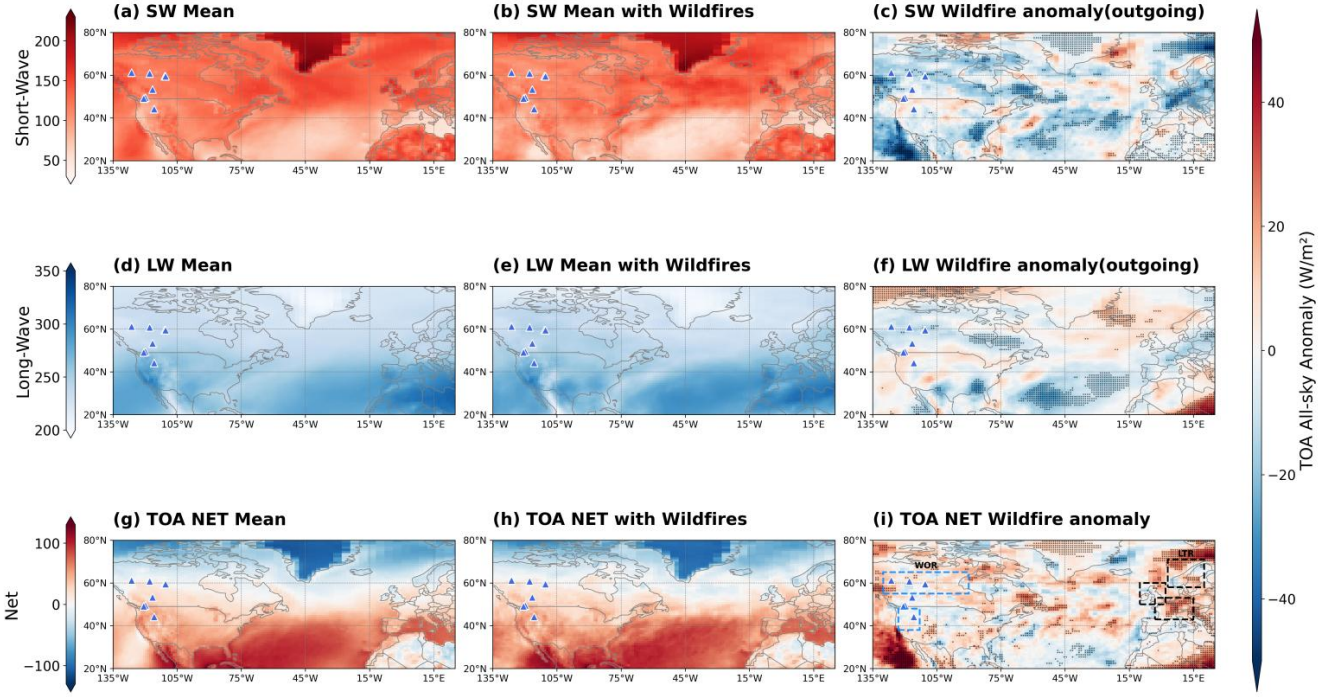

Figure 11. (Figure 6. in the revised manuscript) Wildfires are associated with All-sky TOA radiative Flux Changes. (a-i) Monthly climatological mean TOA radiative fluxes (a, d, g), mean TOA radiative fluxes during Wildfire events (b, e, h) and mean wildfire-associated TOA heat flux anomalies (c, f, i) for SW radiation (a-c), LW radiation (d-f) and Net radiation (g-i). A positive SW anomaly indicates increased outgoing solar radiation or reduced cloud reflection; a positive LW anomaly means more outgoing LW radiation is retained less emitted to space. Net is qualitatively by using SW and LW, but net is calculated independently to remove the seasonal effects of wildfire frequency. Anomalies represent the difference between total events and climatological mean events (Wildfires - Climatology), calculated independently to remove seasonal variations in wildfire events (see in Section 2.3.2). Stippling indicates regions where anomalies are statistically significant at the 95% confidence level based on a 24-year climatology. Blue rectangles show the spatial distribution of identified pyroCb events."

Minor comments:

Lines 96-97: The sentence "These areas were selected based on the spatial distribution of cloud albedo during periods of fire activity as shown by CERES SYN1deg-Month data, in combination with fire hotspots detected by the MODIS Terra" is ambiguous. Could you clarify how cloud albedo was used to select the study areas?

Response:

Thank you for this helpful suggestion. We have clarified the selection criteria for the study areas in the revised manuscript. Specifically, the study areas were identified by calculating the daily anomalies of cloud albedo during the fire periods. Areas exhibiting significant deviations (either higher or lower) compared to the surrounding background and historical averages were selected. This approach allowed us to pinpoint regions where cloud radiative properties were most likely influenced by fire-generated aerosols.

Figure 2a. For clarity, it would be helpful to specify whether the meteorological variables shown in Fig. 2a were averaged over the full fire-intensive region, or only over pixels associated with active fire detections.

Response:

Thank you for this insightful question. We have clarified the methodology in the revised manuscript (Lines 275-276). The meteorological variables presented in Figure 2a were not averaged over the entire geographic rectangle. Instead, they represent the weighted average specifically calculated for pixels associated with active fire detections, as identified by the MOD14A1 fire product. This ensures that the meteorological conditions reflect the actual environment where fire activity was occurring.

Lines 279-281: The local anomalies (T2M +1.45°C, winds +0.5 m/s, low RH, and local vertical uplift) clearly indicate conditions favorable for local ignition and initial fire development. However, regarding the horizontal advection (spread) of the smoke plume, the manuscript does not currently present figures or data showing fire propagation at this stage of the study. Should be included in the next chapter.

Response:

We appreciate this constructive suggestion. In the revised manuscript, we have added comprehensive evidence to characterize the horizontal propagation and advection of the smoke plume:

Refined Trajectory Analysis: We updated Figure 4e-f and added Supplementary Figure S3. These NOAA HYSPLIT forward trajectories are now initialized using the precise pyroCb source locations identified by GOES-16/ABI during the August 2024 events. This provides a direct link between the point-source convective injection and the subsequent long-range horizontal transport.

Meteorological Forcing: Figure 5, showing the horizontal distributions of wind vectors, wind speed, and geopotential height at the SLP, 850 hPa, and 500 hPa. This multi-level analysis demonstrates the synoptic-scale driving forces behind the horizontal advection and dispersion of the smoke plume.

These additions clarify the transition from local ignition to regional-scale propagation, as requested.

Lines 317-318 and Lines 323-324: The manuscript states that "its morphology is similar to the deep convection and upper-level ice clouds commonly observed in PyroCb events" and that "this structure is typical of PyroCb clouds during the decay phase of their transport." For clarity, it would be helpful to cite studies or observational evidence supporting this characterization.

Response: We agree with the reviewer's suggestion to provide more rigorous support for our characterization of the cloud morphology. In the revised manuscript (Lines 317-318 and 323-324), we have incorporated citations of classic and recent studies (Fromm et al., 2010b; Katich et al., 2023b; Peterson et al., 2022) that describe the typical deep-convective and ice-rich structures of PyroCb events. Furthermore, we have cited Kablick III et al., 2020 and Peterson et al., 2022 to support our classification of the observed structure as being representative of the decay and transport phase, where the initial convective core dissipates into a persistent, aerosol-laden ice

cloud.

The revised manuscript text addressing this point is provided below for clarity.

[Revised manuscript text:]

Lines 325-327: "Its morphology is similar to the deep convection and upper-level ice clouds commonly observed in PyroCb event (Fromm et al., 2010; Katich et al., 2023; Peterson et al., 2022)."

Lines 333-334: "This structure is typical of PyroCb during the decay phase of their transport, when only high-altitude ice crystals remain, between 45° N and 65° N(Kablick III et al., 2020; Peterson et al., 2022)"

Figure 4c, d. Given that the CPR vertical profiles in Figure 3 suggest cloud tops reaching the stratosphere, it would be helpful if the authors could explain the rationale for selecting the relatively low altitudes (3, 5, and 7 km a.g.l.) in the NOAA HYSPLIT forward trajectories study.

Response:

We thank the reviewer for pointing out this inconsistency. We agree that the initial altitudes (3, 5, and 7 km) did not fully represent the deep convective injection characterized by the PyroCb events. In response, we have revised the trajectory initialization heights to be strictly consistent with the cloud-top and smoke injection altitudes inferred from the CPR/EarthCARE radar reflectivity and ATLID/EarthCARE Cloud Top Height vertical profiles shown in Figure 3 c-e.

Specifically, the updated forward trajectories were initialized at altitudes corresponding to the observed convective cores and cloud tops: 8 and 11 km AGL for the 23:10 UTC injection, and 7.5 and 10 km AGL for the 23:50 UTC injection on 13 August. These revised altitudes better capture the stratospheric and upper-tropospheric transport pathways of the smoke plume, as suggested by the reviewer.

The revised manuscript text addressing this point is provided below for clarity.

[Revised manuscript text:]

"

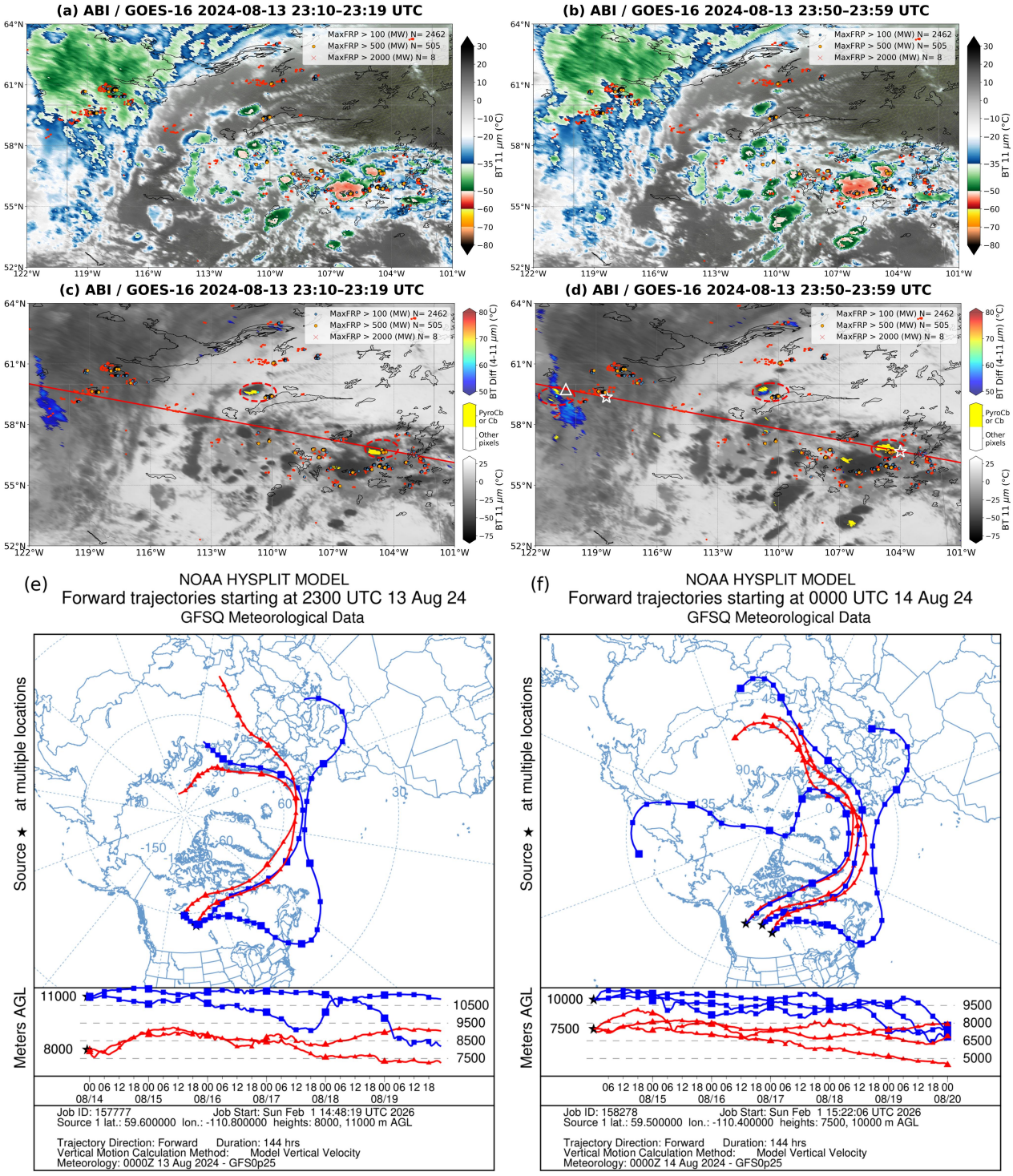

Figure 4. (Figure 7. in the revised manuscript) ABI/GOES-16 observations of cloud-top evolution and smoke transport associated with the 13 August 2024 North American pyroCb events. (a-b) Brightness temperature at 11 μm (BT11) and (c-d) brightness temperature difference between 4 and 11 μm (BTD4-11) derived from GOES-16/ABI on 13 August 2024. Red dots denote MOD14A1 active fire detections, and yellow shaded areas indicate the identified intense pyrocumulonimbus (IPCB) source regions. The pink circle represents the 50 km radius used for pyroCb statistical analysis, with the cyan dot marking the circle center. Red lines show the cross-sections on 13 August in Figure 6. White triangle and stars show vertical pressure velocities of less than -0.4 Pa s^{-1} and high CO concentrations, respectively. (e-f) NOAA HYSPLIT Forward trajectories of air parcels released from the pyroCb source regions on 13-14 August 2024 and transported to the downwind smoke conveyor region. (a,c,e) Region 1 at 59.6°N, 110.8°W and Region 2 at 56.4°N, 104.7°W, with trajectories

initialized at 23:00 UTC on August 13 and arriving at the target region by 23:00 UTC on August 19. (b,d,f) Region 1 at 59.5°N, 110.4°W , Region 2 at 56.8°N, 104.6°W and Region 3 at 59.5°N, 120.95°W, with trajectories initialized at 00:00 UTC on August 14 and arriving at the target region by 00:00 UTC on August 20. "

Lines 377-378: It is somewhat difficult to establish a clear link between the PyroCb source over Oregon (Figure 4) and the plume analyzed in Figures 5a and 6a along the red line (further north); it would be helpful if the authors could clarify whether these plumes originate from a different PyroCb event. Additional labeling or guidance on the source points in Figure 4 could aid interpretation."

Response:

We appreciate the reviewer's request for stronger observational evidence supporting the PyroCb characterization. In response, we have updated Figure 4 to include the EarthCARE ground tracks (red lines) for the 13 August overpass. This visualization confirms that the satellite explicitly intersected two active PyroCb source regions: Region 1 (56.8°N, 104.6°W) and Region 2 (59.5°N, 120.95°W).Furthermore, we have linked these geographic locations to the vertical profiles in Figure 6. Specifically, the strong vertical ascent (vertical pressure velocity -0.4 Pa s-1, marked by white triangle) and enhanced Carbon Monoxide (CO) concentrations (marked by white stars) spatially coincide with Region 2. This coupling of intense ground emissions with vertical transport reflects the rapid injection of fire-generated pollutants into the middle troposphere via convective uplift pathways(Fromm et al., 2010; Kablick III et al., 2020; Peterson et al., 2018).

Figure 8 and 9: Could you please clarify whether this corresponds to a geographical (spatial) average computed over the blue region in Figure 2d?

Response: Thank you for the insightful question. We would like to clarify that the data presented in Figures 8 and 9 are indeed geographical (spatial) averages computed over the high-latitude North American region (NA, 55°–65°N, 130°–90°W), which is indicated by the blue rectangle in Figure 1.

To make this clearer for the readers, we have revised the captions of Figure 8 and Figure 9 as follows: *"The data represent a spatial average over the North American wildfire source region (NA, 55°-65°N, 130°-90°W), as demarcated by the blue rectangle in Figure 1.".*

Repetition in line 475: "influence cloud microphysical characteristics" restates earlier points; it likely

means "macro-physical" (e.g., cover, lifetime) to distinguish from microphysics.

Response:

Thank you for your careful reading and for pointing out this error. We entirely agree with your assessment. The intended meaning was indeed to contrast "microphysical properties" with "macrophysical characteristics" (such as cloud cover and lifetime), as suggested by the observed rise in cloud fraction. I have corrected "microphysical**" to "**macro-physical**".**

Line 490: "The strongest negative anomalies occur over WE (-7.07 ± 0.22 W m^{-2}) and NA (-4.48 ± 0.08 W m^{-2}), consistent with heavy smoke loading in the source regions". But WE is not a source region?

Response: We thank the reviewer for identifying this inaccuracy. We agree that WE is not a primary source region but rather a region impacted by long-range transported wildfire emissions (as defined in our study), whereas NA serves as a major source region.

We have revised the sentence to clearly distinguish between the source region (NA) and the receptor region (WE) impacted by transport. The text now reads:

Revised text: "The most pronounced negative anomalies occur over IGB (-9.63 ± 1.38 W m^{-2}) and NA (-5.07 ± 0.27 W m^{-2}), consistent with heavy smoke loading in the source region (NA) and the accumulation of transported aerosols in the downwind region (IGB).".

Lines 496-497: "These results demonstrate that direct aerosol absorption dominates in the source regions, while aerosol–cloud interactions modulate the SW radiative response in transported plumes." "demonstrate" seems too strong. I would replace with suggest or indicate.

Response: We appreciate the reviewer's suggestion to tone down the statement. We agree that "demonstrate" might be too strong in this context. We have replaced "demonstrate" with "suggest" to more accurately reflect the nature of our findings.

Revised text: *"Consequently, these results suggest that while direct absorption may dictate the clear-sky response, ACI acts as a pivotal modulator under cloudy conditions, driving a net cooling (negative SW anomaly) effect across both source and downwind regions."*

Figure 12: SW CRE and L CRE, wouldn't the plus and minus signs in the corresponding text be reversed?

Response: We thank the reviewer for pointing out this sign inconsistency. The error arose because we applied the standard net flux definition ($F_{net,all}$ - $F_{net,clear}$) directly to the outgoing fluxes

provided by the CERES dataset. Since outgoing flux is defined as upward (positive), this inadvertently reversed the signs of the Cloud Radiative Effect (CRE).

We have corrected the calculation logic to: CRE = $F_{clear}\uparrow$ - $F_{all}\uparrow$. Consequently, Figure 12 has been updated to correctly show negative values for SW CRE (cooling effect) and positive values for LW CRE (warming effect). The corresponding text has also been revised to match these physical conventions.

References

Fromm, M., Lindsey, D.T., Servranckx, R., Yue, G., Trickl, T., Sica, R., Doucet, P., Godin-Beekmann, S., 2010. The Untold Story of Pyrocumulonimbus. https://doi.org/10.1175/2010BAMS3004.1

Kablick III, G.P., Allen, D.R., Fromm, M.D., Nedoluha, G.E., 2020. Australian PyroCb Smoke Generates Synoptic-Scale Stratospheric Anticyclones. Geophysical Research Letters 47, e2020GL088101. https://doi.org/10.1029/2020GL088101

Katich, J.M., Apel, E.C., Bourgeois, I., Brock, C.A., Bui, T.P., Campuzano-Jost, P., Commane, R., Daube, B., Dollner, M., Fromm, M., Froyd, K.D., Hills, A.J., Hornbrook, R.S., Jimenez, J.L., Kupc, A., Lamb, K.D., McKain, K., Moore, F., Murphy, D.M., Nault, B.A., Peischl, J., Perring, A.E., Peterson, D.A., Ray, E.A., Rosenlof, K.H., Ryerson, T., Schill, G.P., Schroder, J.C., Weinzierl, B., Thompson, C., Williamson, C.J., Wofsy, S.C., Yu, P., Schwarz, J.P., 2023. Pyrocumulonimbus affect average stratospheric aerosol composition. Science 379, 815–820. https://doi.org/10.1126/science.add3101

Peterson, D.A., Campbell, J.R., Hyer, E.J., Fromm, M.D., Kablick, G.P., Cossuth, J.H., DeLand, M.T., 2018. Wildfire-driven thunderstorms cause a volcano-like stratospheric injection of smoke. npj Clim Atmos Sci 1, 30. https://doi.org/10.1038/s41612-018-0039-3

Peterson, D.A., Thapa, L.H., Saide, P.E., Soja, A.J., Gargulinski, E.M., Hyer, E.J., Weinzierl, B., Dollner, M., Schöberl, M., Papin, P.P., Kondragunta, S., Camacho, C.P., Ichoku, C., Moore, R.H., Hair, J.W., Crawford, J.H., Dennison, P.E., Kalashnikova, O.V., Bennese, C.E., Bui, T.P., DiGangi, J.P., Diskin, G.S., Fenn, M.A., Halliday, H.S., Jimenez, J., Nowak, J.B., Robinson, C., Sanchez, K., Shingler, T.J., Thornhill, L., Wiggins, E.B., Winstead, E., Xu, C., 2022. Measurements from inside a Thunderstorm Driven by Wildfire: The 2019 FIREX-AQ Field Experiment. https://doi.org/10.1175/BAMS-D-21-0049.1